The Journal of Chemical Physics

Polymer brush-induced depletion interactions and clustering of membrane proteins

Cite as: J. Chem. Phys. **154**, 214901 (2021); https://doi.org/10.1063/5.0048554
Submitted: 24 February 2021 • Accepted: 17 May 2021 • Published Online: 02 June 2021

Anvy Moly Tom, Won Kyu Kim and Changbong Hyeon

The Journal of Chemical Physics ARTICLE scitation.org/journal/jcp

Polymer brush-induced depletion interactions and clustering of membrane proteins

Cite as: J. Chem. Phys. 154, 214901 (2021); doi: 10.1063/5.0048554
Submitted: 24 February 2021 • Accepted: 17 May 2021 •
Published Online: 2 June 2021

Anvy Moly Tom, Won Kyu Kim,[a] and Changbong Hyeon[b]

AFFILIATIONS

Korea Institute for Advanced Study, Seoul 02455, South Korea

Note: This paper is part of the JCP Special Topic on Depletion Forces and Asakura–Oosawa Theory.
[a]**Author to whom correspondence should be addressed:** wonkyukim@kias.re.kr
[b]**Electronic mail:** hyeoncb@kias.re.kr

ABSTRACT

We investigate the effect of mobile polymer brushes on proteins embedded in biological membranes by employing both Asakura–Oosawa type of theoretical model and coarse-grained molecular dynamics simulations. The brush polymer-induced depletion attraction between proteins changes non-monotonically with the size of brush. The depletion interaction, which is determined by the ratio of the protein size to the grafting distance between brush polymers, increases linearly with the brush size as long as the polymer brush height is shorter than the protein size. When the brush height exceeds the protein size, however, the depletion attraction among proteins is slightly reduced. We also explore the possibility of the brush polymer-induced assembly of a large protein cluster, which can be related to one of many molecular mechanisms underlying recent experimental observations of integrin nanocluster formation and signaling.

I. INTRODUCTION

In the 1950s, Asakura and Oosawa (AO) proposed a simple theoretical model to explain the interaction of entropic origin between colloidal particles immersed in a solution of macromolecules,[1,2] which is of great relevance to our understanding of organization and dynamics in a cellular environment. According to the AO theory, rigid spherical objects immersed in the solution of smaller hard spheres representing the macromolecules are expected to feel fictitious attraction, termed depletion force. While the interaction energy of the system remains unchanged, the spherical objects can be attracted to each other. Bringing the large spherical objects into contact can increase the free volume accessible to the smaller hard spheres comprising the medium, hence increasing the total entropy of the hard sphere system ($\Delta S > 0$). The free energy reduction due to the gain in entropy is

$$\Delta F_{\mathrm{HS}} = -T\Delta S = -\left(\frac{3}{2}\lambda + 1\right)\phi k_{\mathrm{B}}T, \tag{1}$$

where λ is the size ratio of large to small hard spheres and ϕ is the volume fraction of small spheres comprising the surrounding medium.[1,3,4] For a fixed value of ϕ, the disparity in size between colloidal particles (large spheres) and macromolecular depletants (small spheres), characterized with the parameter λ, is the key determinant of the magnitude of depletion free energy.[5] The effect of crowding environment on the aggregation of colloidal particles becomes substantial when $\lambda \gg 1$. The cellular environment is highly crowded such that 30% of the cytosolic medium is filled with macromolecules, rendering the interstitial spacing between macromolecules comparable to the average size of proteins ~4 nm.[6] More specifically, this volume fraction of the *Escherichia coli* mixture is contributed by 11% of ribosome, 11% of RNA polymerase, and 8% of soluble proteins.[7] In the cellular environment, the depletion force is one of the fundamental forces of great importance.

The basic principle of the AO theory on rigid bodies with spherical symmetry is straightforward; however, application of the idea to the repertoire of biological and soft materials requires quantitative assessment of *entropy*, which is nontrivial, especially when crowders are characterized with a non-spherical shape and/or with polydispersity[8–12] and when the system is under a special boundary condition.[13,14] For the past few decades, there has also been much interest toward understanding of the effects of crowding in biology,[3,15–19]

which includes crowding-induced structural transitions in disordered chiral homopolymers,[20,21] protein/RNA folding,[22–29] gene regulation through DNA looping,[30] genome compaction,[31] efficient search of proteins for targets on DNA,[32] and molecular motors.[33,34] Furthermore, it is worth mentioning a series of efforts to understand the dynamics of active matter in the language of depletion forces.[35–39]

Besides the examples of depletion force-induced dynamics that all occur in three dimensional space, the AO theory can be extended to lateral depletion effects on the objects whose motion is confined in flat surfaces.[40,41] For a biological membrane where the area fraction of membrane-embedded proteins is as high as 15%–30%, the formation of protein clusters or nano- or microdomains[42–46] is of great relevance to understanding the regulation of biological signal transduction and cell-to-cell communication. Although other physical mechanisms are still conceivable, lateral depletion interactions between membrane embedded proteins can arise from the fluctuations of lipids[40,47,48] or other polymer-like components comprising the fluid membrane,[49,50] contributing to protein–protein attraction and clustering. In this context, the formation of integrin nanodomain enables cell-to-cell communications via signaling,[51–54] particularly the bulky glycocalyx-enhanced integrin clusterings and the associated signaling-induced cancer metastasis observed by Paszek *et al.*[42] make the brush polymer-induced depletion interaction between membrane proteins and their clustering a topic of great relevance to investigate: Paszek *et al.* found that the nanometer scale integrin clusters were induced only by the long and bulky glycocalyx polymers,[42] which are often thought to exert mechanical force to clusters.[55]

Motivated by the above observation, here we study the lateral depletion interactions between rigid inclusions embedded in the mobile polymer brushes on a two-dimensional (2D) surface in the spirit of the AO theory in its simplest form. We compare the results from our simulations with our theoretical predictions. By analyzing the distribution of brush polymer-enhanced protein clusters obtained from our simulations, we attempt to link the brush-size dependent populations of giant protein clusters with the strength of signal transduction observed in the measurement of Paszek *et al.*

II. THEORY: BRUSH-INDUCED LATERAL DEPLETION INTERACTIONS

As illustrated in Fig. 1(a), we consider flexible polymer brushes, each consisting of $N+1$ monomers of size (diameter) b. One end of the individual chain is grafted to the surface but is free to move. If the grafting density σ is large enough to satisfy $\sigma R_F^2 > 1$[56–58] or, equivalently, if the grafting distance (ξ) is smaller than $R_F = bN^{3/5}$, i.e., $\xi < R_F$, where R_F is the Flory radius of the polymer in a good solvent, each polymer reorganizes into a string of self-avoiding blobs due to excluded volume interactions with the neighboring polymers, forming a polymer brush of height H where N/g blobs of size ξ consisting of g segments fill the space above the surface [Fig. 1(a)].[56] In this case, the grafting density $\sigma = N_b/A$, the number of polymer chains (N_b) grafted on an area A, is related to the blob size (or the grafting distance) as $\sigma \simeq 1/\xi^2$. It is straightforward to show using the blob argument that the brush height H scales with N and σ as[56,59,60]

$$H = N\sigma^{1/3}b^{5/3}. \tag{2}$$

Our interest is in the lateral depletion force between two cylindrical inclusions embedded in the polymer brush system, when the two inclusions, constrained to move in xy plane, are separated by a fixed distance r [Figs. 1(b) and 1(c)]. In the presence of the cylindrical inclusions, the volume accessible to the individual polymer chains is determined as follows, depending on r:

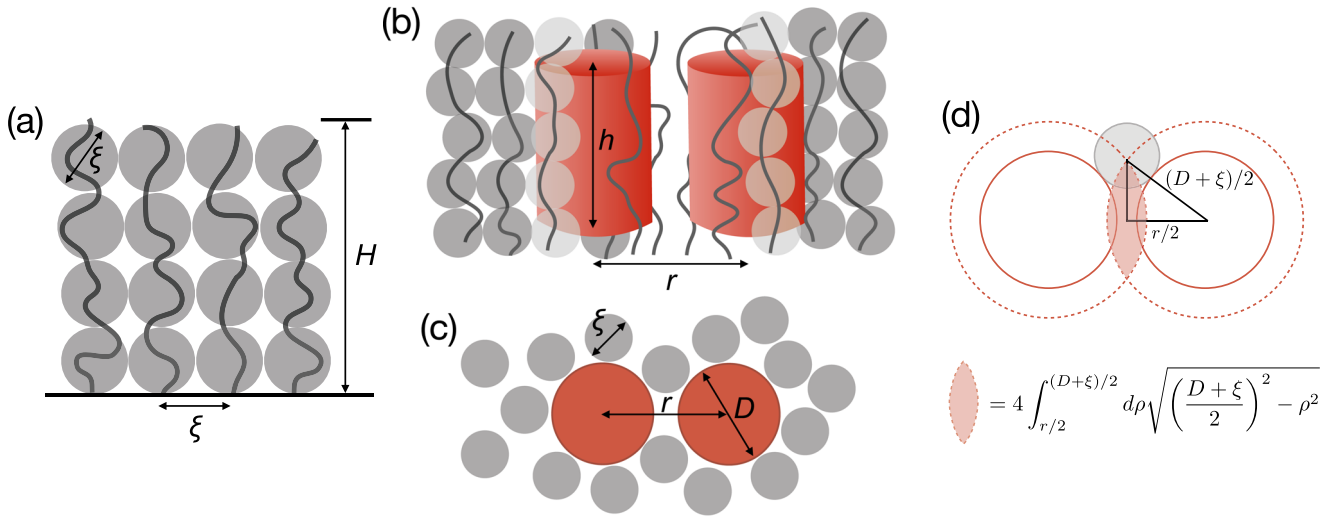

FIG. 1. Brush-induced depletion interactions. (a) Illustration of brush polymers, each of which is organized into a string of blobs of size ξ above the surface. (b) Two cylindrical inclusions (red) separated by the distance r surrounded by brush polymers (gray). (c) Top view of (b). The lateral dimension of the brush polymer ξ corresponds to the size of a blob depicted with gray spheres [see (a)]. (d) Diagram to calculate the brush-induced depletion interaction between the two cylindrical objects. The area inside the dashed line, corresponding to $2\pi[(D+\xi)/2]^2 - A_{\text{overlap}}(r)$ in Eq. (3), is the area inaccessible to the blob of polymer brush of size ξ. The shaded region in pale red is the overlapping area of the two discs of radius $(D+\xi)/2$, separated by the distance r.

$$V(r) = \begin{cases} AH - \left[2\pi\left(\frac{D+\xi}{2}\right)^2 - A_{\text{overlap}}(r)\right]q(h,H) & \text{for } D \le r \le D+\xi \\ AH - 2\pi\left(\frac{D+\xi}{2}\right)^2 q(h,H) & \text{for } r > D+\xi. \end{cases} \tag{3}$$

Here, $A_{\text{overlap}}(r)$ is the overlapping area between two circular discs of radius $(D+\xi)/2$, the region demarcated in pale red in Fig. 1(d),

$$A_{\text{overlap}}(r) = 4\int_{r/2}^{(D+\xi)/2}\left[\left(\frac{D+\xi}{2}\right)^2 - \rho^2\right]^{1/2} d\rho. \tag{4}$$

This is maximized when $r = D$, and its value can be written in terms of the area defined by the square of the grafting distance, ξ^2, multiplied with a dimensionless factor $\chi(\lambda_{\text{br}})$,

$$A_{\text{overlap}}(D) = \xi^2 \underbrace{(1+\lambda_{\text{br}})\int_{\frac{\lambda_{\text{br}}}{1+\lambda_{\text{br}}}}^{1}(1-x^2)^{1/2}dx}_{\equiv\chi(\lambda_{\text{br}})}, \tag{5}$$

where

$$\chi(\lambda_{\text{br}}) = \frac{1}{2}\left[(1+\lambda_{\text{br}})^2\cos^{-1}\left(\frac{\lambda_{\text{br}}}{1+\lambda_{\text{br}}}\right) - \lambda_{\text{br}}\sqrt{1+2\lambda_{\text{br}}}\right]$$
$$\simeq \begin{cases} \frac{\pi}{4} + \frac{\pi-2}{2}\lambda_{\text{br}} + \mathcal{O}(\lambda_{\text{br}}^2) & \text{for } \lambda_{\text{br}} \ll 1 \\ \frac{2\sqrt{2}}{3}\sqrt{\lambda_{\text{br}}} & \text{for } \lambda_{\text{br}} \gg 1 \end{cases}$$

is a monotonically increasing function of $\lambda_{\text{br}} = D/\xi \simeq D\sqrt{\sigma}$, the ratio of the diameter of the inclusions to the grafting distance (or the blob size). Next, the function $q(h,H) \equiv H\Theta(h-H) + h\Theta(H-h)$, defined with the step function, signifies (i) $q(h,H) = H$ when the brush height (H) is shorter than the height of the inclusion (h) ($H < h$) and (ii) $q(h,H) = h$ when the brush is grown over the inclusion ($H > h$) [see Fig. 2(a)]. It is assumed that when $H > h$, the volume above the inclusions, $A \times (H-h)$, is fully accessible to the polymer chains, which is a reasonable assumption when $H \gg h$. Furthermore, under an assumption of no correlation between the polymer chains, which ignores the inter-chain interactions, the partition function for the brush system in the presence of the 2D inclusions separated by r is $Z(r) = [V(r)]^{N_b\times(N+1)}$, where N_b is the number of polymers consisting the brush. The thermodynamic equilibrium is attained by maximizing the total entropy of the system or minimizing the free energy $\beta F(r) = -\log Z(r) = -N_b(N+1)\log V(r)$.

In calculating the partition function, we ignore the correlation (excluded volume interaction) between the brush polymers. In fact, this amounts to the procedure taken in the original version of the AO theory,[1,2] in which the crowders (depletants) repel from colloidal particles (inclusions) but behave like ideal gas particles to each other with no correlation (e.g., excluded volume interaction). Depletion force arising between colloidal particles maximizes the accessible volume for crowders and hence the entropy of the entire system. While there are a number of studies that take into account the inter-crowder correlations by means of adapting the "scaled particle theory,"[61–63] here we stick to the original idea of the AO theory to discuss the key feature of brush polymer-induced depletion interaction.

The gain in free energy due to depletion attraction can be obtained by taking the difference after and before the inclusions are in full contact with each other as $\beta\Delta F = \beta F(D) - \beta F(r \ge D+\xi)$ (see Appendix A for an alternative derivation using the depletion force),

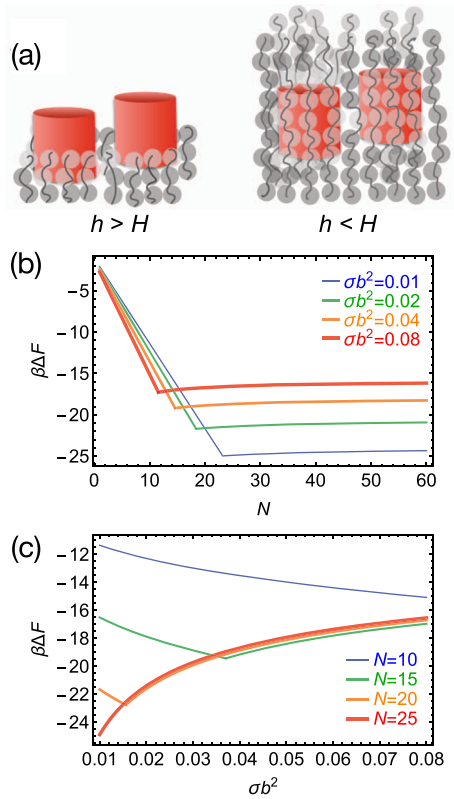

FIG. 2. (a) Two different cases of brush-induced depletion interaction: $h > H$ (left) and $h < H$ (right). (b) and (c) Free energy gain due to brush-induced depletion interaction. Equation (6) was calculated as a function of N for varying σ (b) and as a function of grafting density (σ) for varying N (c), with a cylindrical inclusion at a fixed diameter $D = 5b$ and height $h = 5b$.

$$
\begin{aligned}
-\beta\Delta F &= N_b(N+1)\log\frac{V(D)}{V(r\geq D+\xi)}\\
&= N_b(N+1)\log\left(1+\frac{A_{\text{overlap}}(D)q(h,H)}{AH-2\pi\left(\frac{D+\xi}{2}\right)^2 q(h,H)}\right)\\
&\approx N_b(N+1)\frac{\xi^2\chi(\lambda_{\text{br}})q(h,H)}{AH}\\
&= (N+1)\chi(\lambda_{\text{br}})\frac{q(h,H)}{H}\\
&= \begin{cases}(N+1)\chi(\lambda_{\text{br}}) & \text{for } h>H\\ (N+1)\chi(\lambda_{\text{br}})\dfrac{h}{H} & \text{for } h<H,\end{cases}
\end{aligned}
\tag{6}
$$

where a large volume ($AH \gg 1$) was assumed for the brush system, with $A_{\text{overlap}}(D) = \xi^2\chi(\lambda_{\text{br}})$ and $\sigma\xi^2 \simeq 1$. Equation (6) suggests that N and λ_{br} (or σ) are the key parameters that determine the free energy gain upon brush-induced clustering.

According to Eq. (6) plotted against N in Fig. 2(b), the brush-induced depletion interaction, quantified in terms of stability gain $-\beta\Delta F$, increases linearly with the polymer length ($-\beta\Delta F \propto N$) when the brush is kept shorter than the height of the inclusion ($H < h$). However, as soon as the brush height exceeds the inclusion height ($H > h$), the free energy gain is reduced. When $H > h$, the same amount of accessible volume $A(H-h)$ is added regardless of the state of the two inclusions, increasing both the volume $V(D)$ and $V(r \geq D+\xi)$ accessible for brush polymers. This leads to the reduction of $-\beta\Delta F$. The factor h/H that appears in the last line of Eq. (6) quantifies the extent of this reduction in free energy gain (see Appendix B for further clarification).

For $H \gg h$, the free energy gain converges to

$$
-\beta\Delta F \sim \frac{\chi(\lambda_{\text{br}})h}{\sigma^{1/3}b^{5/3}} < \chi(\lambda_{\text{br}})N, \tag{7}
$$

where the inequality holds because of $h < H = N\sigma^{1/3}b^{5/3}$. In addition, in the limit of $H \gg h$, it can be shown that $-\beta\Delta F \sim \sigma^{-1/12}h$, which explains the σ-dependent limit of $\beta\Delta F$ at large N in Fig. 2(b). The crossover point of the polymer length N^* changes with the grafting density as $N^* \simeq h\sigma^{-1/3}b^{-5/3}$.

There is a crossover in the stability gain as well when the grafting density (σ) is increased [Fig. 2(c)]. The depletion free energy scales with σ as

$$
-\beta\Delta F \sim \begin{cases}(N+1)\sigma^{1/4} & \text{for } \sigma<\sigma^*\\ \dfrac{N+1}{N}\sigma^{-1/12} & \text{for } \sigma>\sigma^*,\end{cases}
\tag{8}
$$

with the crossover grafting density $\sigma^* b^2 \simeq (h/Nb)^3$.

III. NUMERICAL RESULTS

To complement the theoretical argument and predictions given in Sec. II, we perform coarse-grained molecular simulations by explicitly modeling brush polymers and proteins on the 2D surface. The details of models considered in simulations are different from those of the theoretical model, which will be described below. However, the key feature discovered in theory, i.e., the non-monotonic dependence of depletion interactions between a pair of proteins (inclusions) on the brush polymer size N, is confirmed in the simulations.

A. Model

The system is defined by N_{b} brush polymers comprising the brush and M membrane proteins embedded in the brush on the 2D surface (Fig. 3). The center of the protein, modeled as a sphere whose diameter (or vdW radius) is $D = 5a$, is constrained on the surface at $z = D/2$, with a harmonic potential, to move only in parallel to the surface. The individual polymer consisting of N segments (or $N+1$ monomers) is modeled using an energy potential for a bead-spring chain with self-avoidance. Each monomer with diameter a is connected via the harmonic potential

$$
V_{\text{s}}(r_{i,i+1}) = \frac{k_{\text{s}}}{2}(r_{i,i+1}-b)^2, \tag{9}
$$

where $k_{\text{s}} = 3000k_{\text{B}}T/a^2$ is the spring constant and $b = 2^{1/6}a$ is the equilibrium bond length. Similarly to the protein, the first monomers of the chain, grafted to the surface at $z = a/2$, are free to move in the xy plain but constrained in the z direction via a harmonic potential. Any non-grafted monomer whose distance from

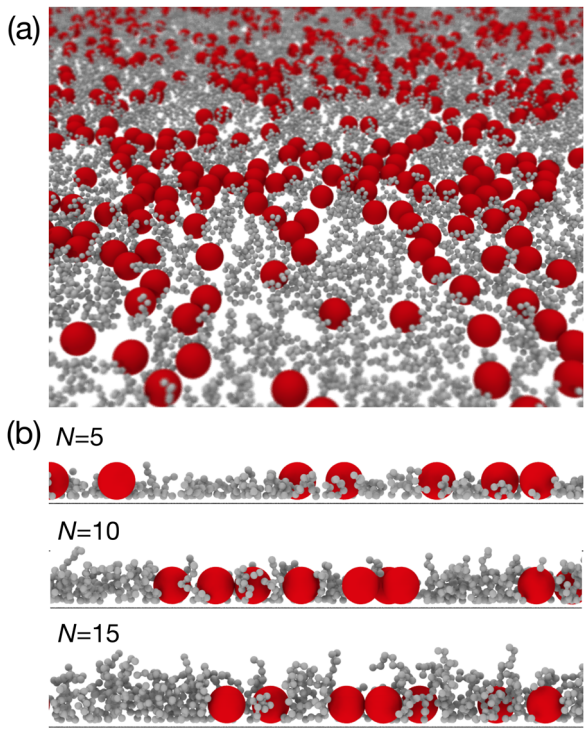

FIG. 3. (a) A snapshot of simulations. The spheres (red) and polymers (gray) represent membrane proteins and brush polymers grafted on the 2D surface, respectively. (b) Lateral view of simulations for different brush sizes (N = 5, 10, and 15).

the grafting surface is $z \le a$ is repelled by the Lennard-Jones (LJ) potential truncated at $z = a$,

$$V_{\mathrm{LJ}}^{\mathrm{surf}}(z) = \begin{cases} 4k_{\mathrm{B}}T\left[\left(\frac{a}{z}\right)^{12} - \left(\frac{a}{z}\right)^{6}\right] & \text{for } z \le a \\ 0 & \text{for } z > a. \end{cases} \tag{10}$$

Both intra-chain and inter-chain monomer–monomer interactions as well as protein–monomer and protein–protein interactions are modeled with the LJ potential

$$V_{\mathrm{LJ}}^{\alpha\beta}(r_{ij}) = \begin{cases} 4\epsilon_{\alpha\beta}\left[\left(\frac{d_{\alpha\beta}}{r_{ij}}\right)^{12} - \left(\frac{d_{\alpha\beta}}{r_{ij}}\right)^{6}\right] & \text{for } r_{ij} \le r_c \\ 0 & \text{for } r_{ij} > r_c. \end{cases} \tag{11}$$

Here, α and β denote different particle types, $\alpha, \beta \in \{\mathrm{m}, \mathrm{P}\}$, with m and P standing for monomer and protein, respectively. r_{ij} is the distance between particles i and j, $\epsilon_{\alpha\beta}$ is the strength of the interaction, and $d_{\alpha\beta}(= (d_\alpha + d_\beta)/2)$ is the contact distance between the particle types α and β. We have chosen $\beta\epsilon_{\alpha\beta} = 1.0$ for all possible pairs of particle types; $d_{\mathrm{P}} = 5a$, $d_{\mathrm{m}} = a$; $r_c = 2.5 \times d_{\mathrm{PP}}$, d_{mP}, and d_{mm} are the values of the cutoff distance for protein–protein, monomer–protein, and monomer–monomer pairs, respectively. As a result, monomer–protein and monomer–monomer interactions are purely repulsive, and the protein–protein interactions in the absence of polymer brush are effectively under the Θ-solvent condition to yield a nearly vanishing second virial coefficient [$B_2 \approx 0$; see Eq. (13)].

The simulation box has a dimension of $L_x = L_y = 200a$ and $L_z = (N+1)b + \Delta$ with $\Delta = 5a$, where a is the basic length unit of our simulations. The system is periodic along the x and y directions and finite in the z direction. With the fixed number of proteins $M = 400$, the area fraction of the membrane proteins is $\phi_{\mathrm{P}} = \pi(D/2)^2 M/(L_x L_y) = 0.2$, which corresponds to the surface density, $\sigma_{\mathrm{P}} = 0.01/a^2$. ϕ_{P} is related to σ_{P} as $\phi_{\mathrm{P}} = \sigma_{\mathrm{P}} \times \pi(D/2)^2$. The grafting density of the brush polymer is calculated using $\sigma = N_{\mathrm{b}}/(L_x L_y - \pi(D/2)^2 M)$. In the simulations, σa^2 is varied between 0.05 and 0.09.

B. Simulations

For the efficient sampling of the configurations of the polymer brush system including proteins, we used the low-friction Langevin dynamics to integrate the equation of motion[64,65]

$$m\ddot{x}_i = -\gamma\dot{x}_i - \partial_{x_i} V(\{\mathbf{r}_k\}) + \eta_i(t), \tag{12}$$

where m is the mass of the ith particle. The characteristic time of the equation is set to $\tau = (ma^2/\epsilon)^{1/2}$ with the characteristic energy scale of inter-particle interaction $\epsilon = 1k_{\mathrm{B}}T$ specified in the energy potential $V(\{\mathbf{r}_k\})$. Then, the friction constant is set to $\gamma = 0.05m/\tau$. The last term $\eta_i(t)$ acting on the ith particle ($i \in \{\mathrm{m}, \mathrm{P}\}$) is the Gaussian white noise with zero mean, $\langle \eta_i(t) \rangle = 0$, satisfying the fluctuation dissipation theorem, $\langle \eta_i(t)\eta_j(t') \rangle = 2\gamma k_{\mathrm{B}}T\delta_{ij}\delta(t-t')$. The equation of motion [Eq. (12)] was integrated using the velocity-Verlet algorithm with the integration time step $\delta t = 0.0025\tau$.[64,65] After the pre-equilibration that fully randomizes the initial configurations of the system, the production runs of 4×10^8 time steps were performed and collected for the statistical analysis.

C. Second virial coefficient

The radial distribution function $g(r)$ between the membrane proteins (see Fig. S1 in the supplementary material) is associated with the second virial coefficient and is calculated for different set of parameters of the brush size (N) and grafting density (σ) as follows:

$$\begin{aligned} B_2 &= \frac{1}{2}\int (1 - e^{-\beta u(\mathbf{r})})\mathrm{d}\mathbf{r} \\ &\simeq \pi \int_0^\infty (1 - g(r))r\mathrm{d}r. \end{aligned} \tag{13}$$

We denote the second virial coefficient of a protein-only system as B_2^{ref} and assess the depletion interaction in terms of $\Delta B_2 = B_2 - B_2^{\mathrm{ref}}$, which can be related to the depletion-induced free energy stabilization as $\beta\Delta F \sim \Delta B_2 \sigma_{\mathrm{P}}\sigma$. To simplify our interpretation of the simulation result, we have chosen the parameters for the protein–protein interaction to yield $B_2^{\mathrm{ref}} \simeq 0$ (see Fig. S2 in the supplementary material).

Overall trends of the simulation results indicate that the depletion interaction between the proteins increases with the increasing grafting density (σ) and brush size (N); however, this trend is saturated or even inverted when the brush size is greater than a certain value (Fig. 4). The non-monotonic dependence of the depletion interaction (ΔB_2) on N becomes more pronounced at high grafting density. Figure 4 shows that the depletion effect for $\sigma a^2 = 0.09$ is maximized at $N = N^* \simeq 10$, at which the brush height (H) becomes comparable to the size of protein (D). This behavior is in agreement with the theoretical prediction of crossover at $h \simeq H = N^*\sigma^{1/3}b^{5/3}$ [Fig. 2(b)]. With $h = 5a$, $\sigma a^2 = 0.09$, and $b = 2^{1/6}a$, we obtain $N^* = h\sigma^{-1/3}b^{-5/3} \simeq 9.2$ (see also Fig. S3 in the supplementary material), which is in good agreement with Fig. 4. This demonstrates that despite the difference in representing proteins, the non-monotonic dependence of brush-induced depletion interactions on the brush

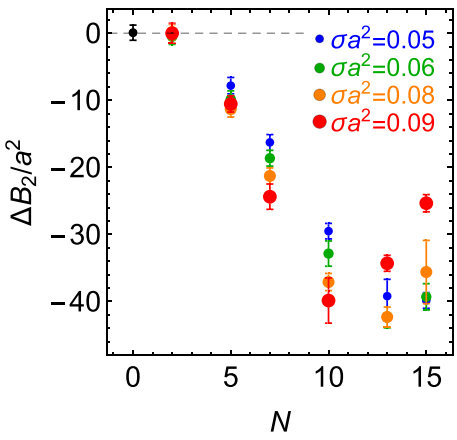

FIG. 4. The measure of the brush polymer-induced protein–protein interaction, $\Delta B_2 = B_2 - B_2^{\mathrm{ref}}$, as a function of the polymer brush size (N) for different grafting densities (σ). The data point at $N = 0$ is for the protein-only reference system.

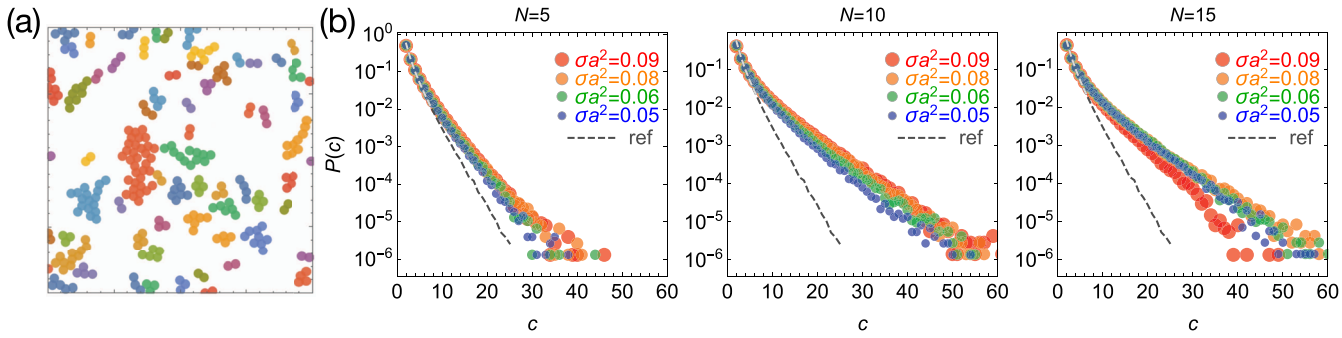

FIG. 5. Cluster size distribution. (a) A snapshot from simulation carried out with $N = 10$, $\sigma_P a^2 = 0.01$, and $\sigma a^2 = 0.09$. (b) The cluster size distribution, $P(c)$, with $\sigma_P a^2 = 0.01$ for varying brush sizes ($N = 5$, 10, and 15) and grafting densities (σ). The dashed lines represent $P_{ref}(c)$, the cluster size distribution for the protein-only system.

polymer size N, predicted by the AO theory extended for brush system, is still captured by the simulations, which complements our theoretical argument.

D. Brush-induced protein clustering

One of the goals of this study is to identify the condition that yields a large sized protein clustering. To this end, we analyze the snapshots of simulations to calculate the cluster size distribution. We consider that two membrane proteins form a cluster of size two if the distance between them is less than the distance criterion of $6a$, which can be extended to identify a cluster of size c. From a number of experimental studies,[42,53,66] it is known that ligand binding to the integrin cluster occurs cooperatively with a large Hill coefficient, and the signaling intensity is proportional to the size of integrin clusters. To this end, we hypothesize that there is a threshold size of integrin clusters (c^*) for the downstream signaling.

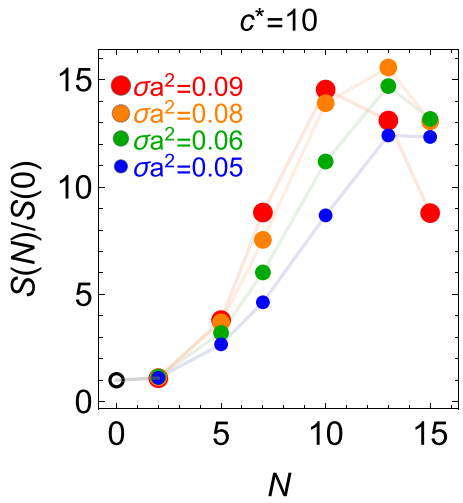

FIG. 6. The intensity of signaling $S(N;\sigma)$ normalized by $S(N = 0)$ (circle) is calculated based on Eq. (14), as a function of the brush size (N) for different grafting densities (σ) with the threshold cluster size $c^* = 10$.

Although the mean cluster size obtained from the simulation results is small ($\langle c\rangle\left[= \int_{c\geq 1} cP(c)\mathrm{d}c\right] = 2 - 3$), the cluster size distributions [$P(c)$] display long tails signifying the presence of large clusters (Fig. 5). Deviation of $P(c)$ from that of the protein-only reference system [$P_{ref}(c)$] is observed at $c \gtrsim c^* \approx 10$ (Fig. 5). With the assumption that the intensity of the downstream signal (S) is proportional to the size of a cluster ($c > c^*$), which is greater than c^*, weighted by the population [$P(c)$], we evaluate the signal relayed from the protein clusters by calculating the mean cluster size above the threshold,

$$S(N,\sigma) \propto \langle c\rangle_> = \int_{c\geq c^*} cP(c;N,\sigma)\mathrm{d}c, \tag{14}$$

with $c^* = 10$. The signal intensity calculated for varying grafting densities (Fig. 6) demonstrates a sigmoidal increase in S as a function of brush size (N) up to $N \leq N^*$, beyond which S decreases, suggestive of the shrinking cluster size, reflecting the decrease in $|\Delta B_2|$. The midpoint of $S(N)$ shifts to a smaller N from $N \simeq 9$ to $N \simeq 6$ as σ increases from $\sigma a^2 = 0.05$ to 0.09.

IV. DISCUSSION

The AO theory extended to the brush system [Eq. (6)] differs from the hard sphere systems with two types (large and small spheres) in three dimensions [Eq. (1)] in several aspects: (i) One of the key parameters $\lambda_{br}(= D/\xi)$ is the ratio of inclusion size (D) to blob size (ξ, grafting distance), whereas $\lambda(= R_L/R_S)$ is the ratio of large to small sphere sizes, R_L and R_S. The blob size ($\xi \simeq bg^{\nu}$), equivalent to the grafting distance, is decided, independently from the size (b) of monomers, via the adaptation of the polymer configuration. The term $\chi(\lambda_{br})$, which is a key determinant of the depletion free energy, is maximized for a larger λ_{br} value under the condition of $H < h$; (ii) $|\beta\Delta F_{HS}| \sim \lambda$, whereas $|\beta\Delta F| \sim \sqrt{\lambda_{br}}$ for $\lambda_{br} \gg 1$; (iii) Whereas $\beta\Delta F_{HS}$, the depletion free energy of the hard sphere system, depends linearly on the volume fraction of crowders ϕ [Eq. (1)], the dependence of area fraction of the brush polymer (or grafting density, σ) is given as $\beta\Delta F \sim \lambda_{br}^{1/2} \sim \sigma^{1/4}$ for $\sigma < \sigma^*$ [Eq. (8)]. (iv) The non-monotonic dependence of depletion free energy on the brush size N is unique to the brush-induced depletion interaction (see Appendix B); such a feature is absent in the hard sphere systems in three dimensions.

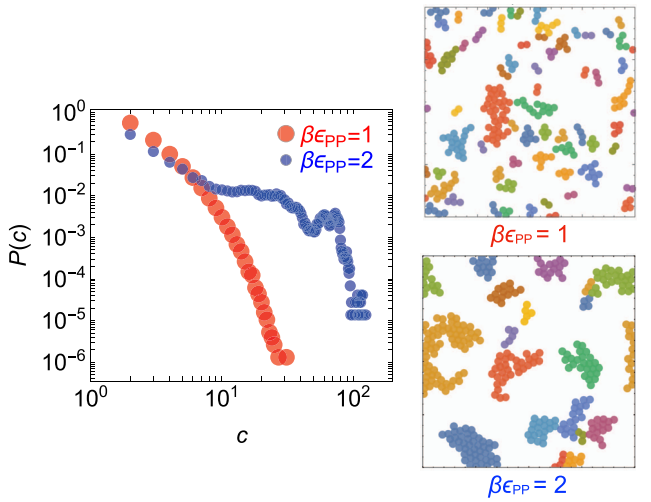

FIG. 7. The cluster size distribution, $P(c)$, for $\beta\epsilon_{PP}$ = 1 and 2. The two panels shown on the right are the snapshots of simulations at $\beta\epsilon_{PP}$ = 1 (top) and 2 (bottom).

The general consensus on the protein clusters on cell surface is that the size of membrane protein assemblies is on the order of ~100 nm.[67,68] On the plasma membrane of T-cells, CD4 proteins form clusters of size varying from 50 to 300 nm.[69] The size of clusters formed by SNARE-protein syntaxin is 50–60 nm, containing 50–75 molecules.[70] This diverse range of the nanocluster domain size may imply various effects that hinder (e.g., due to the bulky extracellular domain of membrane proteins) or promote the cluster formation. Compared with the quantitative knowledge on nanodomains of membrane proteins, the size of protein clusters implicated in Fig. 5(a) is smaller. Besides the brush polymer enhanced assembly of a protein cluster, one can consider other physical mechanisms that increase the effective attraction between proteins, such as inter-protein helix–helix interactions,[71–73] protein sorting via hydrophobic mismatch,[74–76] membrane curvature,[77,78] and thermal Casimir-like long-range force resulting from membrane undulation.[79–81] Upon increasing the LJ potential parameter from $\beta\epsilon_{PP}$ = 1 to $\beta\epsilon_{PP}$ = 2, which lowers the B_2 coefficient below zero and increases the direct protein–protein interaction drastically (Fig. S2 in the supplementary material), the contribution of the tail part of $P(c)$ becomes significant, and a host of large and stable protein clusters are more frequently found (Fig. 7). For $\beta\epsilon_{PP}$ = 2, the protein cluster size could be as large as $m \approx 100$.

V. CONCLUDING REMARKS

We have studied polymer brush-induced entropic force in a system of rigid bodies constrained to move on the surface. Both our theory and simulation results show that the depletion free energy is a non-monotonic function of brush height (H), which is determined by the brush size (N) and surface grafting density (σ). Our theoretical argument explaining the features of lateral depletion force is based on the AO theory, which takes only the volume accessible to individual brush polymers into consideration to calculate the depletion free energy in terms of geometrical factors (N and λ_{br}). Despite its simplicity, which not only represents the proteins with cylinders but also ignores the inter-chain correlations, the main features predicted by our theory concerning the brush-induced depletion interaction are in qualitative agreement with the simulation results. The basic theoretical idea presented in this work, which models the brush polymers with flexible self-avoiding chains, may be further extended to explore the effects of brush polymers with different rigidities and morphologies on the protein clustering.[53,82]

The size of protein clusters assembled due to the brush-induced depletion interaction is slightly smaller than that estimated from measurements, which requires other factors. Our study reiterates that along with aforementioned membrane-undulation-induced protein clustering,[79–81] the brush-induced depletion interaction is one of the important entropic forces that may contribute to bringing an order to the membrane environment.

SUPPLEMENTARY MATERIAL

See the supplementary material for the radial distribution function between the proteins, the second virial coefficients in the protein-only systems, and the mean brush height.

ACKNOWLEDGMENTS

This study was supported by KIAS Individual Grant Nos. CG076001 (W.K.K.) and CG035003 (C.H.). We thank the Center for Advanced Computation in KIAS for providing computing resources.

APPENDIX A: DEPLETION FORCE

The brush-induced 2D depletion force acting on the two objects is $\beta f(r) = -(\partial\beta F/\partial r)_\beta$,

$$\beta f(r) = \frac{N_b(N+1)A'_{overlap}(r)q(h,H)}{AH - \left[2\pi\left(\frac{D+\xi}{2}\right)^2 - A_{overlap}(r)\right]q(h,H)} \tag{A1}$$

for $D \le r \le D+\xi$ and $\beta f(r) = 0$ for $r > D+\xi$. For a very large system [$A \gg 2\pi((D+\xi)/2)^2$], the denominator of Eq. (A1) is dominated by the term AH, and the depletion force for $D \le r \le D+\xi$ simplifies to

$$\beta f(r) = -2\sigma(N+1)\left[\left(\frac{D+\xi}{2}\right)^2 - \left(\frac{r}{2}\right)^2\right]^{1/2}\frac{q(h,H)}{H}, \tag{A2}$$

where the grafting density of the polymer brush $\sigma = N_b/A$ was used. For $r > D+\xi$, $\beta f(r) = 0$. It is noteworthy that the depletion force is always attractive [$f(r) < 0$] for $D \le r \le D+\xi$.

The free energy gain upon aggregation or the work needed to separate the two inclusions in the brush system apart beyond the distance $D+\xi$ is obtained by integrating the depletion force from $r = D$ to $r = D+\xi$, which yields the expression identical to Eq. (6).

APPENDIX B: NON-MONOTONICITY OF DEPLETION FREE ENERGY GAIN WITH INCREASING BRUSH POLYMER SIZE (H)

Here, we clarify how the non-monotonic change of $-\beta\Delta F$ arises with increasing H, starting from the expression of the free energy gain ($-\beta\Delta F$) given in the first line of Eq. (6),

$$-\beta\Delta F \sim \frac{N_b H}{\sigma^{1/3}} \log \frac{V(D)}{V(r \geq D+\xi)}. \tag{B1}$$

To begin, we define a_c as the area occupied by the inclusions when they are in contact and a as the area occupied by the inclusions when they are separated beyond $r = D + \xi$. Other parameters N_b, H, h, and A are already defined in the main text. Below, we use the condition that the overlapping area $A_{\text{overlap}}(D) = a - a_c \equiv \delta a$ is small compared to A ($\delta a/A \ll 1$).

(i) For $H < h$,

$$\begin{aligned} -\beta\Delta F &\sim \frac{N_b H}{\sigma^{1/3}} \log \frac{(A-a_c)h}{(A-a)h} \\ &= \frac{N_b H}{\sigma^{1/3}} \log\left[1 + \frac{\delta a}{A-a}\right] \\ &\approx \frac{N_b}{\sigma^{1/3}} \left(\frac{H}{1-a/A}\right) \frac{\delta a}{A} \\ &\approx \frac{1}{\sigma^{1/3}} \left(\frac{H}{1-a/A}\right) \chi(\lambda_{\text{br}}), \end{aligned} \tag{B2}$$

where $\delta a = \xi^2 \chi(\lambda_{\text{br}})$, $N_b/A = \sigma$, and $\sigma\xi^2 \simeq 1$ were used to obtain the expression in the last line. Thus, for $H < h$, $-\beta\Delta F$ increases linearly with H.

(ii) For $H \geq h$,

$$\begin{aligned} -\beta\Delta F &\sim \frac{N_b H}{\sigma^{1/3}} \log \frac{(AH - a_c h)}{(AH - ah)} \\ &= \frac{N_b H}{\sigma^{1/3}} \log\left[1 + \frac{\delta a \times h}{AH - ah}\right] \\ &\approx \frac{N_b}{\sigma^{1/3}} \left(\frac{h}{1-ah/AH}\right) \frac{\delta a}{A} \\ &= \frac{1}{\sigma^{1/3}} \left(\frac{h}{1-ah/AH}\right) \chi(\lambda_{\text{br}}). \end{aligned} \tag{B3}$$

Thus, for $H \geq h$, $-\beta\Delta F$ decreases with H from $-\beta\Delta F = \frac{1}{\sigma^{1/3}}\left(\frac{h}{1-a/A}\right)\chi(\lambda_{\text{br}})$, which is the maximum value of $-\beta\Delta F$, and converges to $(h/\sigma^{1/3})\chi(\lambda_{\text{br}})$ when $H/h \gg 1$.

DATA AVAILABILITY

The data that support the findings of this study are available from the corresponding author upon reasonable request.

REFERENCES

[1] S. Asakura and F. Oosawa, J. Chem. Phys. **22**, 1255 (1954).
[2] S. Asakura and F. Oosawa, J. Polym. Sci. **33**, 183 (1958).
[3] D. Marrenduzzo, K. Finan, and P. R. Cook, J. Cell Biol. **175**, 681 (2006).
[4] C. Jeon, C. Hyeon, Y. Jung, and B.-Y. Ha, Soft Matter **12**, 9786 (2016).
[5] H. Kang, P. A. Pincus, C. Hyeon, and D. Thirumalai, Phys. Rev. Lett. **114**, 068303 (2015).
[6] R. Phillips, J. Kondev, J. Theriot, N. Orme, and H. Garcia, *Physical Biology of the Cell* (Garland Science, New York, 2009).
[7] E. Roberts, A. Magis, J. O. Ortiz, W. Baumeister, and Z. Luthey-Schulten, PLoS Comput. Biol. **7**, e1002010 (2011).
[8] L. Onsager, Ann. N. Y. Acad. Sci. **51**, 627 (1949).
[9] M. Dijkstra and D. Frenkel, Phys. Rev. Lett. **72**, 298 (1994).
[10] Y. Mao, M. E. Cates, and H. N. W. Lekkerkerker, Phys. Rev. Lett. **75**, 4548 (1995).
[11] Y. Mao, M. E. Cates, and H. N. W. Lekkerkerker, J. Chem. Phys. **106**, 3721 (1997).
[12] H. Kang, N. M. Toan, C. Hyeon, and D. Thirumalai, J. Am. Chem. Soc. **137**, 10970 (2015).
[13] P. D. Kaplan, J. L. Rouke, A. G. Yodh, and D. J. Pine, Phys. Rev. Lett. **72**, 582 (1994).
[14] A. D. Dinsmore, D. T. Wong, P. Nelson, and A. G. Yodh, Phys. Rev. Lett. **80**, 409 (1998).
[15] A. P. Minton, Curr. Opin. Struct. Biol. **10**, 34 (2000).
[16] S. R. McGuffee and A. H. Elcock, PLoS Comput. Biol. **6**, e1000694 (2010).
[17] R. J. Ellis, Trends Biochem. Sci. **26**, 597 (2001).
[18] L. Sapir and D. Harries, Curr. Opin. Colloid Interface Sci. **20**, 3 (2015).
[19] B. van den Berg, R. J. Ellis, and C. M. Dobson, EMBO J. **18**, 6927 (1999).
[20] Y. Snir and R. D. Kamien, Science **307**, 1067 (2005).
[21] A. Kudlay, M. S. Cheung, and D. Thirumalai, Phys. Rev. Lett. **102**, 118101 (2009).
[22] H.-X. Zhou, G. Rivas, and A. P. Minton, Annu. Rev. Biophys. **37**, 375 (2008).
[23] A. Elcock, Curr. Opin. Struct. Biol. **20**, 196 (2010).
[24] M. S. Cheung, D. Klimov, and D. Thirumalai, Proc. Natl. Acad. Sci. U. S. A. **102**, 4753 (2005).
[25] D. L. Pincus, C. Hyeon, and D. Thirumalai, J. Am. Chem. Soc. **130**, 7364 (2008).
[26] D. Kilburn, J. H. Roh, L. Guo, R. M. Briber, and S. A. Woodson, J. Am. Chem. Soc. **132**, 8690 (2010).
[27] N. A. Denesyuk and D. Thirumalai, J. Am. Chem. Soc. **133**, 11858 (2011).
[28] A. G. Gasic, M. M. Boob, M. B. Prigozhin, D. Homouz, C. M. Daugherty, M. Gruebele, and M. S. Cheung, Phys. Rev. X **9**, 041035 (2019).
[29] A. Soranno, I. Koenig, M. B. Borgia, H. Hofmann, F. Zosel, D. Nettels, and B. Schuler, Proc. Natl. Acad. Sci. U. S. A. **111**, 4874 (2014).
[30] G.-W. Li, O. G. Berg, and J. Elf, Nat. Phys. **5**, 294 (2009).
[31] J. S. Kim, V. Backman, and I. Szleifer, Phys. Rev. Lett. **106**, 168102 (2011).
[32] C. A. Brackley, M. E. Cates, and D. Marenduzzo, Phys. Rev. Lett. **111**, 108101 (2013).
[33] B. J. N. Reddy, S. Tripathy, M. Vershinin, M. E. Tanenbaum, J. Xu, M. Mattson-Hoss, K. Arabi, D. Chapman, T. Doolin, C. Hyeon *et al.*, Traffic **18**, 658 (2017).
[34] G. Nettesheim, I. Nabti, C. U. Murade, G. R. Jaffe, S. J. King, and G. T. Shubeita, Nat. Phys. **16**, 1144 (2020).
[35] J. Dzubiella, H. Löwen, and C. Likos, Phys. Rev. Lett. **91**, 248301 (2003).
[36] L. Angelani, C. Maggi, M. Bernardini, A. Rizzo, and R. Di Leonardo, Phys. Rev. Lett. **107**, 138302 (2011).
[37] T. Sanchez, D. T. N. Chen, S. J. DeCamp, M. Heymann, and Z. Dogic, Nature **491**, 431 (2012).
[38] R. Ni, M. A. C. Stuart, and P. G. Bolhuis, Phys. Rev. Lett. **114**, 018302 (2015).
[39] L. Huber, R. Suzuki, T. Krüger, E. Frey, and A. R. Bausch, Science **361**, 255 (2018).
[40] T. Sintes and A. Baumgärtner, Biophys. J. **73**, 2251 (1997).
[41] K. Suda, A. Suematsu, and R. Akiyama, J. Chem. Phys. **154**, 204904 (2021).
[42] M. J. Paszek, C. C. DuFort, O. Rossier, R. Bainer, J. K. Mouw, K. Godula, J. E. Hudak, J. N. Lakins, A. C. Wijekoon, L. Cassereau *et al.*, Nature **511**, 319 (2014).
[43] G. J. Bakker, C. Eich, J. A. Torreno-Pina, R. Diez-Ahedo, G. Perez-Samper, T. S. van Zanten, C. G. Figdor, A. Cambi, and M. F. Garcia-Parajo, Proc. Natl. Acad. Sci. U. S. A. **109**, 4869 (2012).
[44] C. Selhuber-Unkel, M. López-García, H. Kessler, and J. P. Spatz, Biophys. J. **95**, 5424 (2008).

[45]T. S. van Zanten, J. Gómez, C. Manzo, A. Cambi, J. Buceta, R. Reigada, and M. F. Garcia-Parajo, Proc. Natl. Acad. Sci. U. S. A. **107**, 15437 (2010).
[46]M. F. Garcia-Parajo, A. Cambi, J. A. Torreno-Pina, N. Thompson, and K. Jacobson, J. Cell Sci. **127**, 4995 (2014).
[47]O. Soubias, W. E. Teague, Jr., K. G. Hines, and K. Gawrisch, Biophys. J. **108**, 1125 (2015).
[48]A. Kusumi and J. S. Hyde, Biochemistry **21**, 5978 (1982).
[49]J. U. Kim and B. O'Shaughnessy, Macromolecules **39**, 413 (2006).
[50]R. K. W. Spencer and B.-Y. Ha, Macromolecules **54**, 1304–1313 (2021).
[51]M. J. Williams, P. E. Hughes, T. E. O'Toole, and M. H. Ginsberg, Trends Cell Biol. **4**, 109 (1994).
[52]L. Kornberg, H. S. Earp, J. T. Parsons, M. Schaller, and R. L. Juliano, J. Biol. Chem. **267**, 23439 (1992).
[53]M. J. Paszek, D. Boettiger, V. M. Weaver, and D. A. Hammer, PLoS Comput. Biol. **5**, e1000604 (2009).
[54]B. Cheng, W. Wan, G. Huang, Y. Li, G. M. Genin, M. R. K. Mofrad, T. J. Lu, F. Xu, and M. Lin, Sci. Adv. **6**, eaax1909 (2020).
[55]G. Marsico, L. Russo, F. Quondamatteo, and A. Pandit, Trends Cancer **4**, 537 (2018).
[56]P. G. de Gennes, Macromolecules **13**, 1069 (1980).
[57]L. Liu, P. A. Pincus, and C. Hyeon, Macromolecules **50**, 1579 (2017).
[58]L. Liu and C. Hyeon, J. Chem. Phys. **149**, 163302 (2018).
[59]S. Alexander, J. Phys. **38**, 983 (1977).
[60]M. Rubinstein, R. H. Colby *et al.*, *Polymer Physics* (Oxford University Press, New York, 2003), Vol. 23.
[61]H. Reiss, H. L. Frisch, and J. L. Lebowitz, J. Chem. Phys. **31**, 369 (1959).
[62]A. P. Minton, Biopolymers **20**, 2093 (1981).
[63]M. Castelnovo and W. M. Gelbart, Macromolecules **37**, 3510 (2004).
[64]T. Veitshans, D. Klimov, and D. Thirumalai, Folding Des. **2**, 1 (1997).
[65]C. Hyeon and D. Thirumalai, J. Am. Chem. Soc. **130**, 1538 (2008).
[66]D. S. Harburger and D. A. Calderwood, J. Cell Sci. **122**, 159 (2009).
[67]T. Lang and S. O. Rizzoli, Physiology **25**, 116 (2010).
[68]F. Baumgart, A. M. Arnold, K. Leskovar, K. Staszek, M. Fölser, J. Weghuber, H. Stockinger, and G. J. Schütz, Nat. Methods **13**, 661 (2016).
[69]T. Lukeš, D. Glatzová, Z. Kvíčalová, F. Levet, A. Benda, S. Letschert, M. Sauer, T. Brdička, T. Lasser, and M. Cebecauer, Nat. Commun. **8**, 1731 (2017).
[70]J. J. Sieber, K. I. Willig, R. Heintzmann, S. W. Hell, and T. Lang, Biophys. J. **90**, 2843 (2006).
[71]N. Ben-Tal and B. Honig, Biophys. J. **71**, 3046 (1996).
[72]J. H. Lorent and I. Levental, Chem. Phys. Lipids **192**, 23 (2015).
[73]V. Anbazhagan and D. Schneider, Biochim. Biophys. Acta, Biomembr. **1798**, 1899 (2010).
[74]U. Schmidt, G. Guigas, and M. Weiss, Phys. Rev. Lett. **101**, 128104 (2008).
[75]D. Milovanovic, A. Honigmann, S. Koike, F. Göttfert, G. Pähler, M. Junius, S. Müllar, U. Diederichsen, A. Janshoff, H. Grubmüller *et al.*, Nat. Commun. **6**, 5984 (2015).
[76]B. West, F. L. H. Brown, and F. Schmid, Biophys. J. **96**, 101 (2009).
[77]H. T. McMahon and J. L. Gallop, Nature **438**, 590 (2005).
[78]B. J. Reynwar, G. Illya, V. A. Harmandaris, M. M. Müller, K. Kremer, and M. Deserno, Nature **447**, 461 (2007).
[79]M. Goulian, R. Bruinsma, and P. Pincus, Europhys. Lett. **22**, 145 (1993).
[80]J.-M. Park and T. C. Lubensky, J. Phys. I **6**, 1217 (1996).
[81]B. B. Machta, S. L. Veatch, and J. P. Sethna, Phys. Rev. Lett. **109**, 138101 (2012).
[82]J. J. Madsen, J. M. A. Grime, J. S. Rossman, and G. A. Voth, Proc. Natl. Acad. Sci. U. S. A. **115**, E8595 (2018).